Supplementary Information (SI) for Dalton Transactions.
This journal is © The Royal Society of Chemistry 2026

Electronic Supplementary Information

Amplified Electron-Spin Thermal Sensitivity in Mn(II) Complexes

Anthony J. Campanella,[a] Amanda Gin,[a] Siyoung Sung,[a] Cassidy E. Jackson,[a] Roxanna Martinez,[b] Ökten Üngör,[b] Srikanth Dasari,[b] Andrew Ozarowski,[c] Indrani Bhowmick,[d] Joseph Zadrozny[b,*]

[a]*Department of Chemistry, Colorado State University, Fort Collins, CO 80523, United States.*
[b]*Department of Chemistry and Biochemistry, The Ohio State University, Columbus, OH 43210, United States.*
[c]*National High Magnetic Field Laboratory, Tallahassee, FL 32310, United States.*
[d]*Analytical Resources Core Facility, Colorado State University, Fort Collins, CO 80523, United States.*
**Corresponding author. Email: zadrozny.13@osu.edu*

Contents

Specific Heat Capacity Fitting Details S2
Table S1. Crystallographic refinement details for **1** S3
Table S2. Crystallographic refinement details for **2** S4
Table S3. Crystallographic refinement details for **3** S5
Table S4. Summary of possible hydrogen-bonding contacts for **1-3** S6
Table S5. Summary of high-frequency/field EPR simulation parameters for **1**. S7
Table S6. Summary of high-frequency/field EPR simulation parameters for **2**. S8
Table S7. Summary of high-frequency/field EPR simulation parameters for **3**. S9
Table S8. Summary of X-band EPR simulation parameters for **1**. S10
Table S9. Summary of X-band EPR simulation parameters for **2**. S11
Table S10. Summary of X-band EPR simulation parameters for **3**. S12
Figure S1. Graphical depictions of the coordination polyhedra in **1-3** S13
Figure S2. Depiction of closest H•••F interactions in **2**. S14
Figure S3. UV-Vis spectral data for **1-3** S15
Figure S4. Room-temperature, solution-phase emission data for **1-3** S16
Figure S5. Variable-temperature magnetic susceptibility data for **1-3** S17
Figure S6. Simulations of 390 GHz spectra with positive/negative *D* and *E* for **1-3** S18
Figure S7. Select variable-temperature 390 GHz solid-state EPR spectra with simulations for **1**. S19
Figure S8. Select variable-temperature 390 GHz solid-state EPR spectra with simulations for **2**. S20
Figure S9. Select variable-temperature 390 GHz solid-state EPR spectra with simulations for **3**. S21
Figure S10. Frozen-solution, variable-temperature X-band EPR spectra for **1** and **3**. S22
Figure S11. Temperature-dependent X-band peak positions for **1** in frozen solution S23
Figure S12. Temperature-dependent X-band peak positions for **2** in frozen solution S24
Figure S13. Temperature-dependent X-band peak positions for **3** in frozen solution S25
Figure S14. Variable-temperature echo-detected Q-band EPR spectra for **2** S26
Figure S15. Temperature-dependent Q-band peak positions for **2** in frozen solution S27
Figure S16. Variable-field heat capacity data and fits for **2** S28
Figure S17. Variable-field heat capacity data and fits for **3** S29
Figure S18. Powder diffraction data and simulations for **1-3** S30

Specific Heat Capacity Fitting Details

Specific heat capacity data were modeled using Equation 1.1, which includes both spin and high-temperature limit Debye contributions.

$$C_p = \frac{Z\left(\sum_{i=1}^{dim} {E_i}^2 e^{\frac{-E_i}{k_B T}}\right) - \left(\sum_{i=1}^{dim} {E_i}^2 e^{\frac{-E_i}{k_B T}}\right)^2}{{k_B}^2 T^2 Z^2} + 9R\left(\frac{T}{\theta_D}\right)^3 \int_0^{\frac{\theta_D}{T}} \frac{x^4 e^x}{(e^x-1)^2} dx \qquad (1.1)$$

$$Z = \sum_{i=1}^{dim} e^{\frac{-E_i}{k_B T}} \qquad (1.2)$$

$$x = \frac{\hbar\omega}{k_B T} \qquad (1.3)$$

where Equation 1.2 is the partition function given the magnetization for a single Cartesian direction in Bohr Magnetons per mole (μ_B mol^{-1})[1], E_i are the energy of states, k_B is the Boltzmann constant, T is temperature (K), θ_D is the Debye temperature (K), $\hbar$ is the reduced Plank's constant, and ω is the frequency of the phonon mode. Heat capacity data were fit in a two-fold manner, first fitting the low-temperature, applied field data using PHI[1] then adding the Debye contribution via scipy.optimize.curve_fit(), as implemented in Python.

(1) N. F. Chilton, R. P. Anderson, L. D. Turner, A. Soncini and K. S. Murray, *J. Comput. Chem.*, 2013, **34**, 1164-1175.

Table S1. Crystallographic information for the structural refinement of **1**.

Empirical formula	$C_{36}H_{60}F_{24}Mn_2N_{16}P_4$
Formula weight	703.38 g/mol
Temperature	99.99 K
Crystal system	Trigonal
Space group	P31c
a	9.5381(2) Å
b	9.5381(2) Å
c	17.2367(6) Å
α	90°
β	90°
γ	120°
Volume	1358.03(7) $Å^3$
Z	1
ρ_{calc}	1.720 g cm^{-3}
μ	0.713 mm^{-1}
F(000)	714
Crystal color	Orange
Crystal size	0.997 × 0.793 × 0.101 mm^3
Radiation	MoKα (λ = 0.71073 Å)
2θ range for data collection	2.363 to 25.673°
Index ranges	$-11 \leq h \leq 11$, $-11 \leq k \leq 11$, $-21 \leq l \leq 21$
Reflections collected	85645
Independent collections	1726 [R_{int} = 0.0688]
Data/restraints/parameters	1726/1/125
Goodness-of-fit on F^2	1.113
Final R indexes [$I \geq 2\sigma(I)$]	R_1 = 0.0260, wR_2 = 0.0677
Final R indexes [all data]	R_1 = 0.0277, wR_2 = 0.0687
Largest diff. peak/hole	0.42/-0.19 e $Å^{-3}$
Absolute structure parameter	0.49(3)

Table S2. Crystallographic refinement details for the structural refinement of **2**.

Empirical formula	$C_{18}H_{42}F_{12}MnN_8P_2$
Formula weight	715.48 g/mol
Temperature	100 K
Crystal system	Trigonal
Space group	P–31c
a	9.7469(4) Å
b	9.7469(4) Å
c	16.8886(13) Å
α	90°
β	90°
γ	120°
Volume	1389.50(16) $Å^3$
Z	2
ρ_{calc}	1.710 g cm^{-3}
μ	0.698 mm^{-1}
F(000)	738
Crystal color	Orange
Crystal size	0.178 × 0.114 × 0.111 mm^3
Radiation	MoKα (λ = 0.71073 Å)
2θ range for data collection	2..412 to 31.494°
Index ranges	$-14 \leq h \leq 14$, $-14 \leq k \leq 14$, $-24 \leq l \leq 24$
Reflections collected	154430
Independent collections	1560 [R_{int} = 0.0609, R_{sigma} = 0.0085]
Data/restraints/parameters	1559/0/64
Goodness-of-fit on F^2	1.056
Final R indexes [$I \geq 2\sigma(I)$]	R_1 = 0.0237, wR_2 = 0.0641
Final R indexes [all data]	R_1 = 0.0269, wR_2 = 0.0663
Largest diff. peak/hole	0.44/-0.34 e $Å^{-3}$

Table S3. Crystallographic refinement details for the refinement of **3**.

Empirical formula	$C_{24}H_{34}F_{12}MnN_4O_4P_2$
Formula weight	787.43 g/mol
Temperature	100 K
Crystal system	Monoclinic
Space group	*P*–1
a	9.7907(8) Å
b	16.4512(13) Å
c	19.0904(17) Å
α	87.804(3) °
β	89.891(3)°
γ	89.806(2)°
Volume	3072.6(4) $Å^3$
Z	4
ρ_{calc}	1.702 g cm^{-3}
μ	0.646 mm^{-1}
F(000)	1604
Crystal color	Colorless block
Crystal size	0.09 × 0.057 × 0.057 mm^3
Radiation	MoKα (λ = 0.71073 Å)
2θ range for data collection	2.080 to 26.501°
Index ranges	$-12 \leq h \leq 12$, $-20 \leq k \leq 20$, $-23 \leq l \leq 23$
Reflections collected	108979
Independent collections	12616 [R_{int} = 0.0568, R_{sigma} = 0.0315]
Data/restraints/parameters	12616/181/929
Goodness-of-fit on F^2	1.028
Final R indexes [$I \geq 2\sigma(I)$]	R_1 = 0.0362, wR_2 = 0.0811
Final R indexes [all data]	R_1 = 0.0437, wR_2 = 0.0857
Largest diff. peak/hole	0.449/-0.368 e $Å^{-3}$

Table S4. Summary of H-bonding H···F contacts < 2.9 Å for **1-3**.[a]

[MnL1]$(PF_6)_2$ (**1**)	Atom 1 (D)[b]	Atom 2 (A)[b]	D···A (Å)	Angle D–H···A (°)
	$C_{N\text{-imino}}$	F	3.33	123.58
	$C_{\alpha\text{-amino}}$		3.35	132.77
	$C_{N\text{-imino}}$		3.37	155.87
	C_{imino}		3.38	141.09
[MnL2]$(PF_6)_2$ (**2**)	Atom 1 (D)	Atom 2 (A)	D···A (Å)	Angle D–H···A (°)
	N_{amino}	F	3.2	132.99
	N_{amino}		3.28	168.58
	$C_{\alpha\text{-amino}}$		3.52	133.34
	$C_{\alpha\text{-amino}}$		3.53	155.6
[MnL3]$(PF_6)_2$ (**3**)[c]	Atom 1 (D)[d]	Atom 2 (A)	D···A (Å)	Angle D–H···A (°)
	$C_{\alpha\text{-amino}}$	F	3.23	142.92
	$C_{\alpha\text{-O}}$		3.24	126.21
	$C_{2\text{-pyridyl}}$		3.26	170.28
	$C_{\alpha\text{-amino}}$		3.26	144.12

[a]Shortest four unique contacts are given. [b]Subscript definitions:"N-imino" indicates the C atom singly bonded to the N of the imino group. "α-amino" is the alpha carbon to the tertiary amine in the ligand framework. [c]Hydrogen bonding analysis was omitted from disordered PF_6^-. [d]Subscript definitions: α-amino, alpha carbon to tertiary amines; α-O alpha carbon to ether groups; 2-pyridyl: carbon at 2-position of the ligand pyridyl rings.

Table S5. Tabulation of best simulation parameters for the variable-temperature, solid state 390 GHz EPR spectra of **1**.

T	g_x	g_y	g_z	**Strain**[a]	***D*** **(MHz)**	***E*** **(MHz)**
5	2.015	1.995	1.998	[0.011 0.02 0.01]	800	220
10	2.005	2.001	2	[0.01 0.01 0.012]	760	210
20	2.006	2.003	2.002	[0.01 0.008 0.01]	720	210
30	2.006	2.003	2.002	[0.017 0.009 0.014]	700	210
40	2.002	2.0015	2.001	[0.011 0.01 0.01]	700	200
50	2.004	2.002	1.999	[0.009 0.009 0.009]	700	200
60	2.002	2.001	1.995	[0.009 0.009 0.009]	700	200
70	2.003	2.002	1.999	[0.009 0.008 0.009]	700	200
80	2	1.999	1.995	[0.009 0.008 0.009]	700	200
100	2.001	2	1.995	[0.009 0.008 0.009]	700	200
120	2.003	2.002	1.999	[0.007 0.008 0.008]	700	200
140	2.0015	2	1.994	[0.007 0.008 0.008]	700	200
160	2.0035	2.002	1.995	[0.007 0.009 0.009]	700	200
180	2.003	2.001	1.992	[0.007 0.007 0.008]	700	200
200	2.0035	2.0025	2	[0.007 0.007 0.008]	650	200
250	2.003	2.001	1.995	[0.007 0.009 0.008]	650	200
300	2.005	2.004	1.999	[0.007 0.009 0.008]	650	200

[a]Strains used are *g* strains ordered as strain in [g_x g_y g_z]

Table S6. Tabulation of best simulation parameters for the variable-temperature, solid state 390 GHz EPR spectra of **2**.

T	g_x	g_y	g_z	**Strain**[a]	***D*** **(MHz)**	***E*** **(MHz)**
5	1.998	1.999	1.989	[0.02 0.0025 0.007]	900	220
10	1.998	1.999	1.994	[0.02 0.002 0.006]	1070	220
20	2.000	1.997	1.995	[0.02 0.002 0.007]	1090	260
30	2.004	2.0025	2.000	[0.02 0.003 0.006]	1250	360
40	2.0025	2.001	1.999	[0.015 0.007 0.006]	1290	400
50	2.004	2.0037	2.002	[0.015 0.007 0.006]	1340	400
60	2.002	2.001	2.000	[0.015 0.007 0.006]	1340	400
70	2.004	2.0037	2.002	[0.015 0.007 0.008]	1340	400
80	2.0035	2.003	2.002	[0.013 0.007 0.009]	1300	400
100	2.0035	2.003	2.002	[0.014 0.006 0.009]	1340	410
120	2.001	2.001	2.000	[0.014 0.006 0.009]	1280	400
140	2.0035	2.0035	2.0025	[0.013 0.006 0.01]	1280	400
160	2.0015	2.0005	1.999	[0.013 0.006 0.008]	1280	400
180	2.004	2.0035	2.001	[0.013 0.0065 0.008]	1280	400
200	2.002	2.0015	2.000	[0.013 0.007 0.008]	1280	400
250	2.004	2.003	2.003	[0.013 0.009 0.006]	1280	400
300	2.0015	2.0005	2.000	[0.013 0.007 0.006]	1240	380

[a]Strains used are *g* strains ordered as strain in [g_x g_y g_z]

Table S7. Tabulation of best simulation parameters for the variable-temperature, solid state 390 GHz EPR spectra of **3**.

T	g_x	g_y	g_z	**Strain**	***D*** **(MHz)**	***E*** **(MHz)**
5	1.997	2.006	2.001	[0.016 0.009 0.009]	1050	260
10	1.999	2.008	2.003	[0.008 0.008 0.011]	950	230
20	1.996	2.0045	2.001	[0.006 0.006 0.005]	940	200
30	1.996	2.006	2.001	[0.006 0.006 0.005]	940	200
40	1.998	2.008	2.004	[0.006 0.007 0.006]	940	220
50	1.999	2.005	2.001	[0.006 0.006 0.007]	940	220
60	2.000	2.006	2.002	[0.005 0.005 0.006]	940	220
70	1.999	2.0045	2.000	[0.006 0.005 0.006]	940	220
80	2.001	2.0065	2.002	[0.0055 0.005 0.006]	940	220
100	2.001	2.007	2.002	[0.006 0.005 0.006]	940	220
120	2.000	2.005	2.001	[0.006 0.0055 0.006]	940	220
140	2.001	2.006	2.001	[0.006 0.006 0.006]	940	220
160	2.000	2.004	2.000	[0.006 0.006 0.006]	940	220
180	2.001	2.005	2.001	[0.006 0.006 0.006]	940	220
200	2.001	2.005	2.001	[0.006 0.006 0.006]	940	220
250	2.002	2.005	2.002	[0.006 0.006 0.006]	900	220
300	2.000	2.002	2.000	[0.006 0.006 0.006]	900	220

[a]Strains used are *g* strains ordered as strain in [g_x g_y g_z]

Table S8. Tabulation of best simulation parameters for the variable-temperature, frozen solution state 9.36 GHz EPR spectra of **1** in butyronitrile at 5 mM. Units of A and A strain are MHz. [a]Strains used are g and A strains ordered as $[g_x\ g_y\ g_z]$ and $[A_x\ A_y\ A_z]$.

T	g_x	g_y	g_z	g strain[a]	D (MHz)	E (MHz)
5.5	2.049	2.038	2.034	[0.003 0.035 0.002]	800	225
10	2.049	2.042	2.030	[0.003 0.020 0.002]	790	210
20	2.000	1.990	1.980	[0.001 0.040 0.040]	795	220
30	2.000	1.990	1.980	[0.001 0.035 0.035]	810	220
40	2.000	1.995	1.975	[0.001 0.035 0.035]	790	220
50	2.000	1.995	1.975	[0.001 0.035 0.035]	800	215
60	2.000	1.995	1.975	[0.001 0.025 0.025]	800	215

T	A_x	A_y	A_z	A strain[a]
5.5	210	255	210	[55 95 95]
10	215	257	215	[55 85 70]
20	230	220	235	[5 95 85]
30	230	220	235	[5 95 85]
40	230	225	230	[5 95 85]
50	230	225	230	[5 95 85]
60	230	225	240	[5 95 85]

Table S9. Tabulation of best simulation parameters for the variable-temperature, frozen solution state 9.36 GHz EPR spectra of **2** in butyronitrile at 5 mM. Units of *A* and *A*-strain are MHz. [a]Strains used are *g* and *A* strains ordered as [g_x g_y g_z] and [A_x A_y A_z].

T	g_x	g_y	g_z	***g* strain**[a]	***D* (MHz)**	***E* (MHz)**
10	2.007	2.004	2.002	[0.015 0.015 0.015]	1260	220
20	2.007	2.004	2.002	[0.015 0.015 0.015]	1280	220
30	2.007	2.004	2.002	[0.015 0.015 0.015]	1270	215
40	2.007	2.004	2.002	[0.015 0.015 0.015]	1275	210
50	2.007	2.004	2.002	[0.015 0.015 0.015]	1275	210
60	2.007	2.004	2.002	[0.015 0.015 0.015]	1285	210

T	A_x	A_y	A_z	***A* strain**[a]
10	215	240	220	[75 85 85]
20	210	235	215	[75 85 85]
30	215	240	220	[75 85 85]
40	215	240	220	[75 85 85]
50	215	240	220	[75 85 85]
60	215	240	220	[75 85 85]

Table S10. Tabulation of best simulation parameters for the variable-temperature, frozen solution state 9.36 GHz EPR spectra of **3** in butyronitrile at 5 mM. Units of *A* and *A* strain are MHz. [a]Strains used are *g* and *A* strains ordered as [g_x g_y g_z] and [A_x A_y A_z].

T	g_x	g_y	g_z	***g* strain[a]**	***D* (MHz)**	***E* (MHz)**
5.5	2.020	2.015	2.022	[0.002 0.002 0.002]	980	205
10	2.010	2.005	2.012	[0.002 0.002 0.002]	980	220
25	2.010	2.005	2.012	[0.002 0.002 0.002]	975	215
30	2.005	2.005	2.005	[0.002 0.002 0.002]	960	205
40	2.005	2.005	2.005	[0.008 0.008 0.008]	955	210
50	2.005	2.005	2.005	[0.008 0.008 0.008]	945	205
60	2.005	2.005	2.005	[0.008 0.008 0.008]	945	205

T	A_x	A_y	A_z	***A* strain[a]**
5.5	210	200	240	[25 45 15]
10	240	265	245	[25 45 25]
25	235	255	235	[35 45 35]
30	210	275	240	[15 55 15]
40	235	300	265	[80 85 35]
50	230	295	260	[80 85 35]
60	230	295	260	[80 85 35]

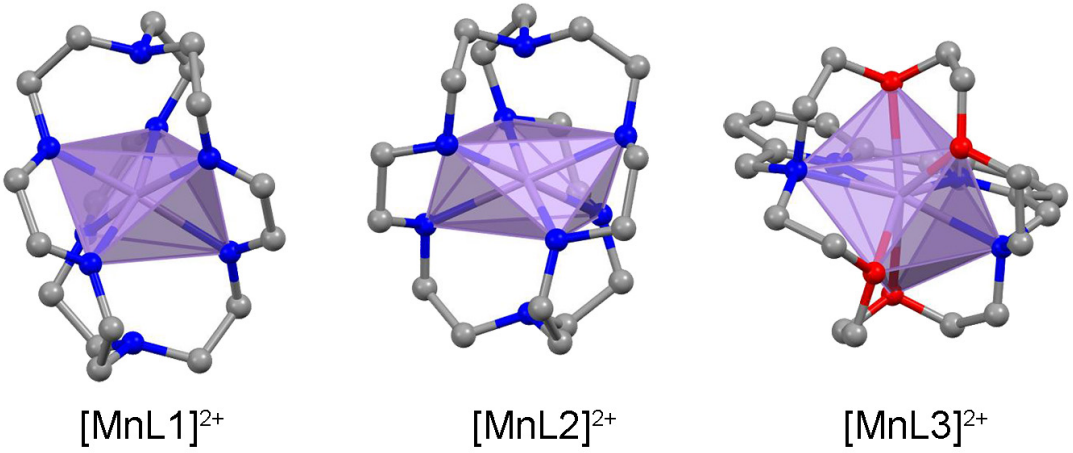

Fig. S1. Depictions of the Mn-centered coordination polyhedra in **1-3**.

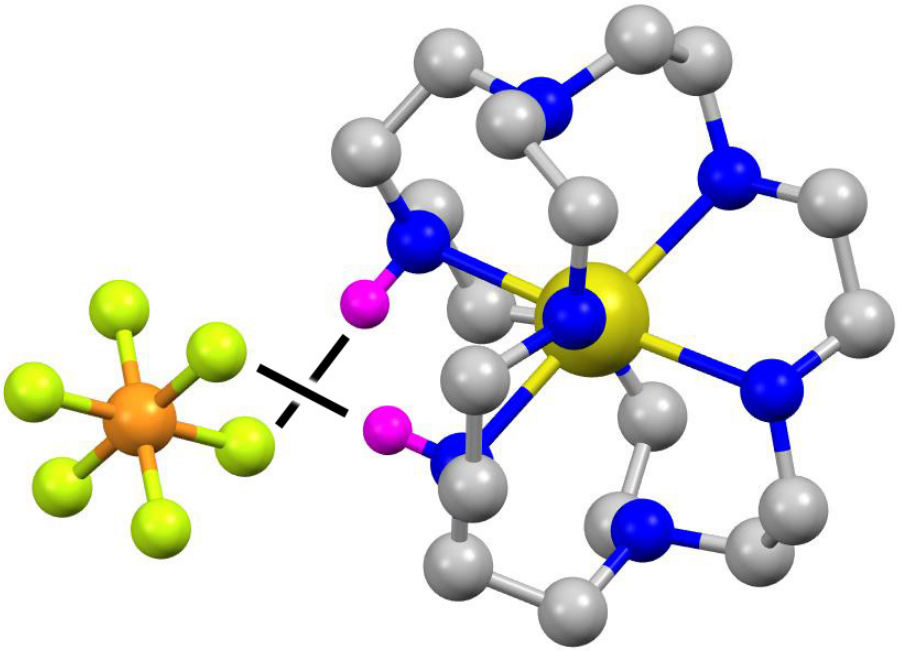

Fig. S2. Depictions of the F•••H interactions between $[MnL2]^{2+}$ and the nearest PF_6^- anion. Of the four H•••F interactions, there are two unique distances: 2.43(1) Å and 2.29(1) Å. Gold, bright yellow-green, orange, blue, gray, and pink spheres represent Mn, F, P, N, C, and H atoms respectively. Non H-bonded hydrogens and the second PF_6^- anion are not shown for clarity.

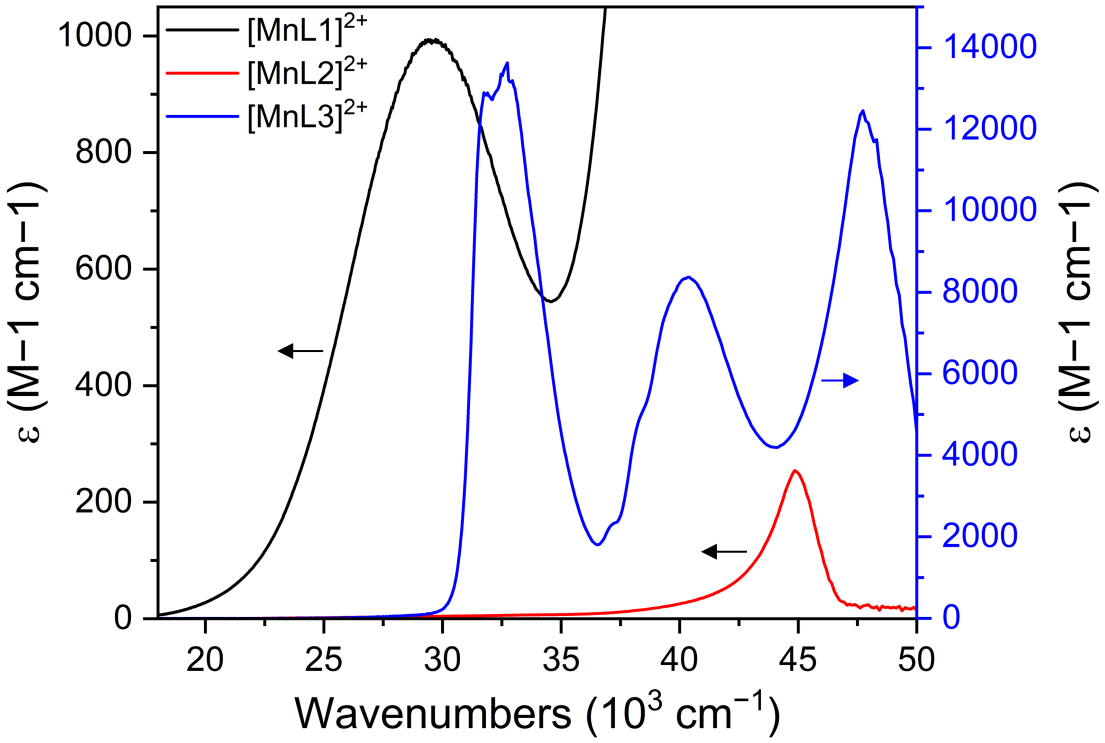

Fig. S3. Solution phase, room temperature UV-Vis spectra for **1**-**3**. Concentrations were *ca*. 0.1 to 10 mM in the complexes. Intensities are normalized to ε values from 3-point Beers' law analyses.

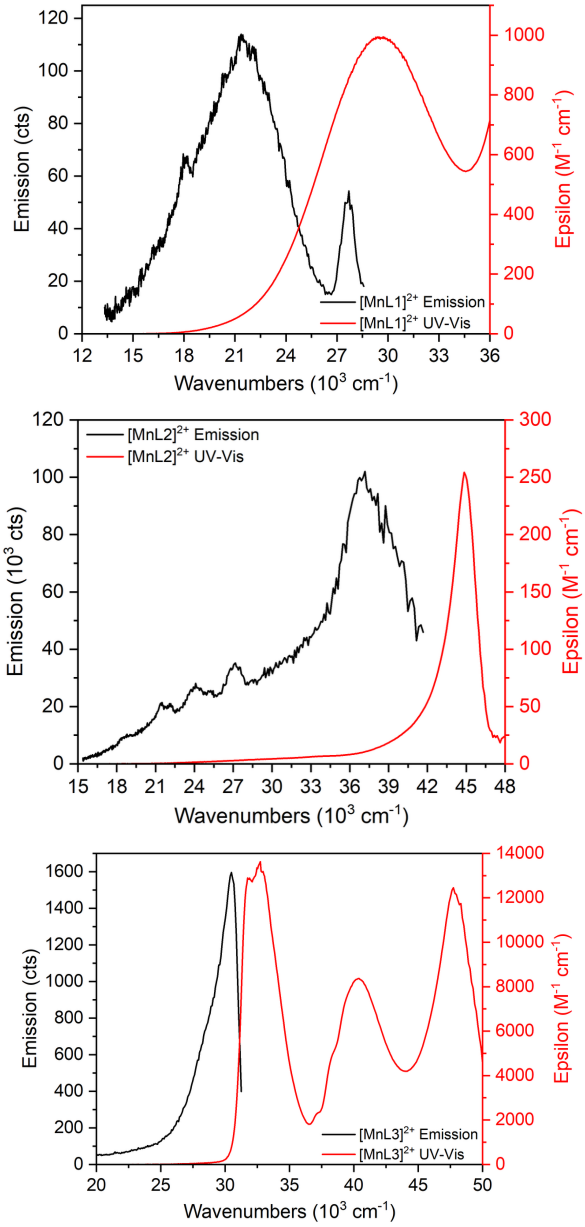

Fig. S4. Solution phase, room temperature Emission spectra for **1** (top), **2** (middle), and **3** (bottom). Irradiation wavelengths were 300 m (**1**), 220 nm (**2**), 300 nm (**3**), with integration times of 0.5 s. Concentrations were 0.2 to 12 mM (same as UV-Vis in Fig. S2), the solvent was MeCN and the temperature of measurement was 20 °C.

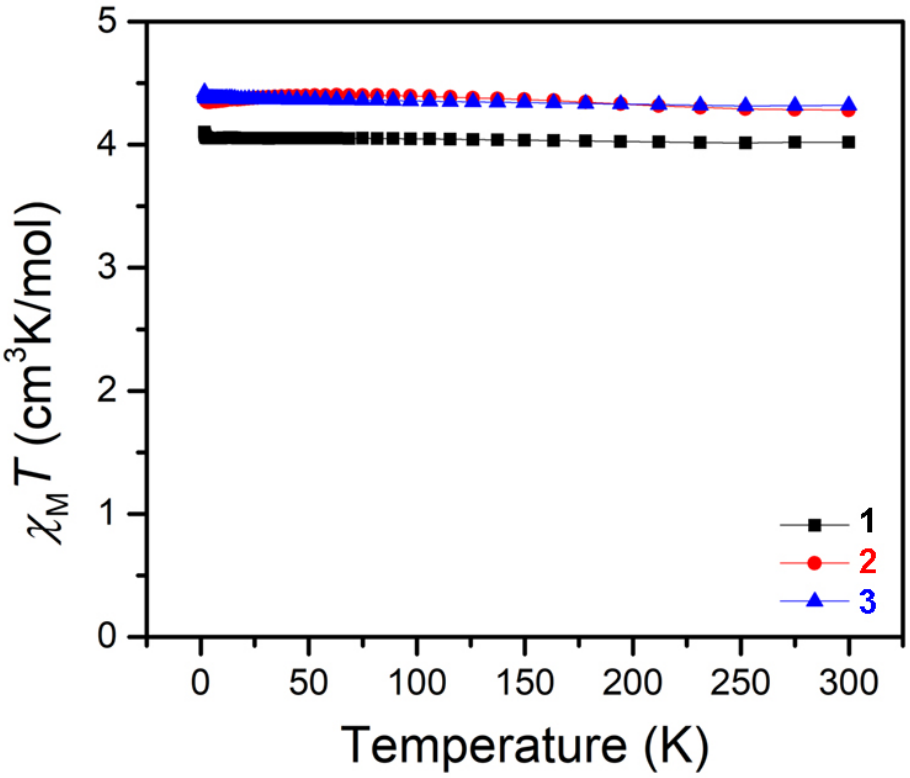

Fig. S5. Variable-temperature dc magnetic susceptibility ($\chi_M T$) for complexes **1-3**. Data were collected under at 1000 G magnetic field on microcrystalline powders. Solid lines are guides for the eye.

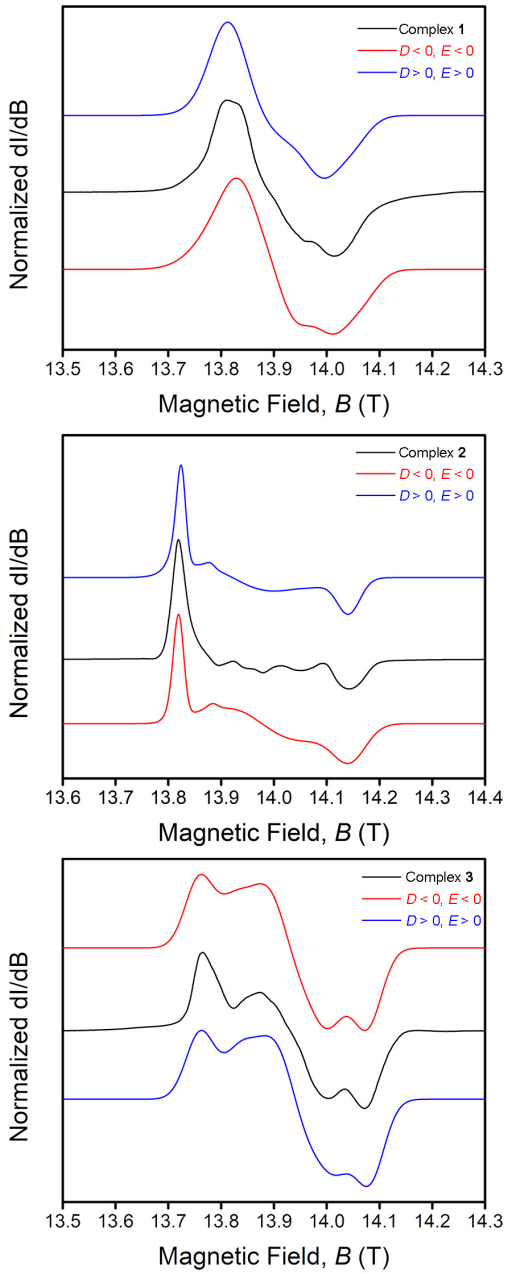

Fig. S6. 5 K, 390 GHz EPR spectra for **1** (top), **2** (middle), and **3** (bottom) with simulations of positive D and E and simulations with negative D and E. Simulation parameters for positive D, E are in Tables S4-S6. Parameters for the negative D and E best simulation of **1** are: [g_x, g_y, g_z] = [2.018 1.996 1.995], g strain = [0.019 0.01 0.01]; D = –800 MHz, E = –220 MHz. Parameters for the negative D and E best simulation of **2** are: [g_x, g_y, g_z] = [1.996 1.986 1.997], g strain = [0.019 0.01 0.003]; D = –910 MHz, E = –210 MHz. Parameters for the negative D and E best simulation of **3** are: [g_x, g_y, g_z] = [2.001 1.997 2.003], g strain = [0.016 0.009 0.009]; D = –1050 MHz, E = –240 MHz.

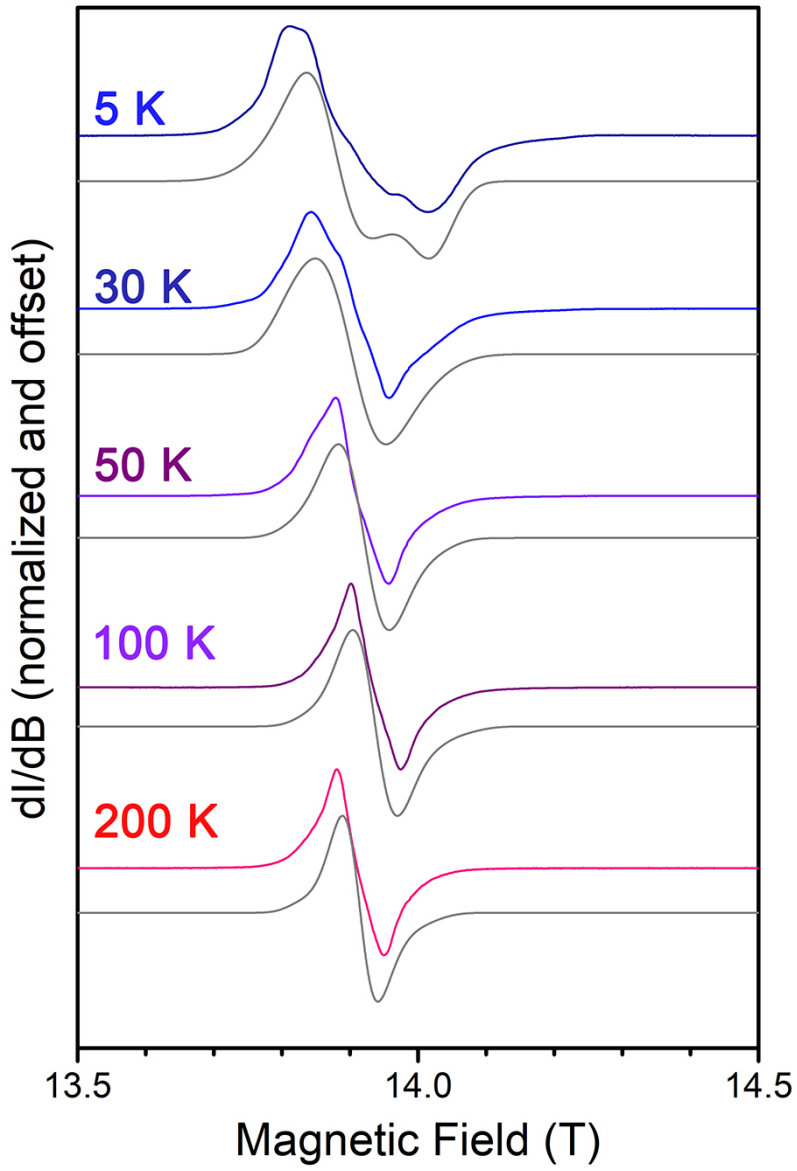

Fig. S7. Select variable-temperature 390 GHz solid-state EPR spectra for **1**. Colored lines correspond to the temperatures indicated on the graph. Gray lines are best simulations. Parameters for these simulations are listed in Table S4 and see the main manuscript for discussion.

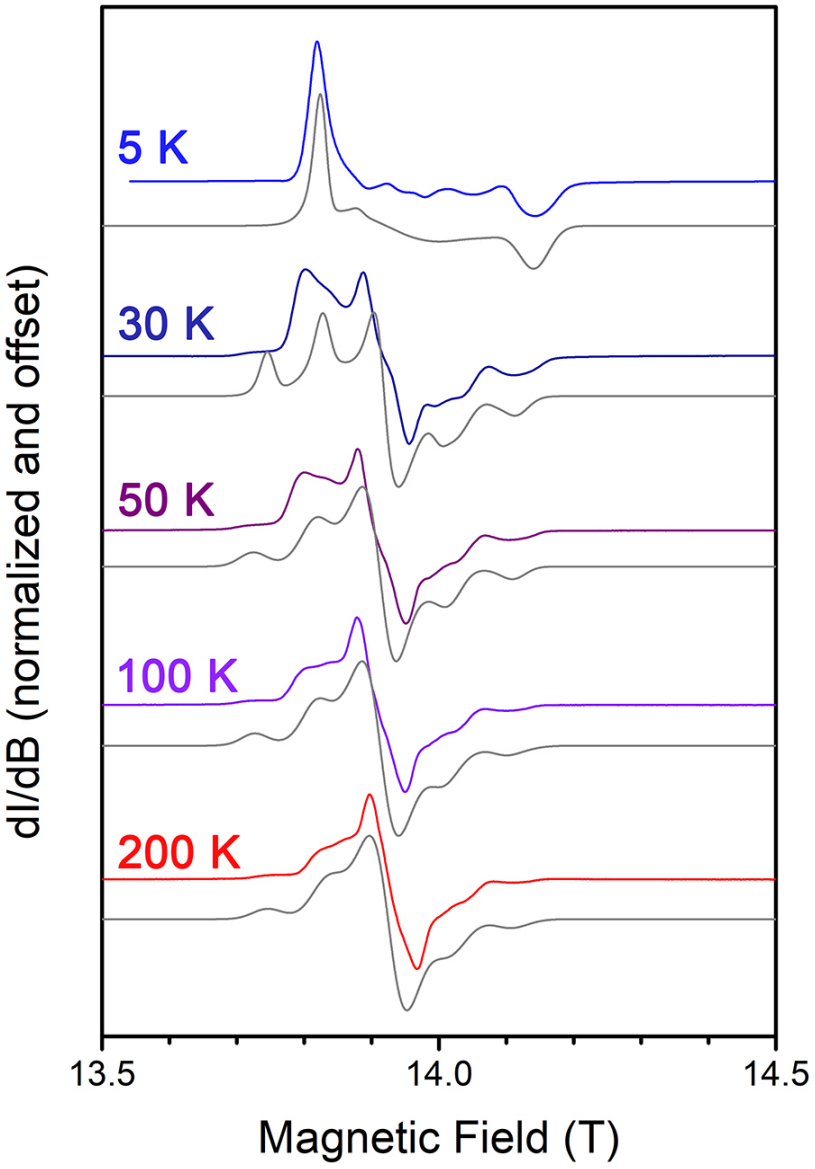

Fig. S8. Select variable-temperature 390 GHz solid-state EPR spectra for **2**. Colored lines correspond to the temperatures indicated on the graph. Gray lines are best simulations. Parameters for these simulations are listed in Table S5 and see the main manuscript for discussion.

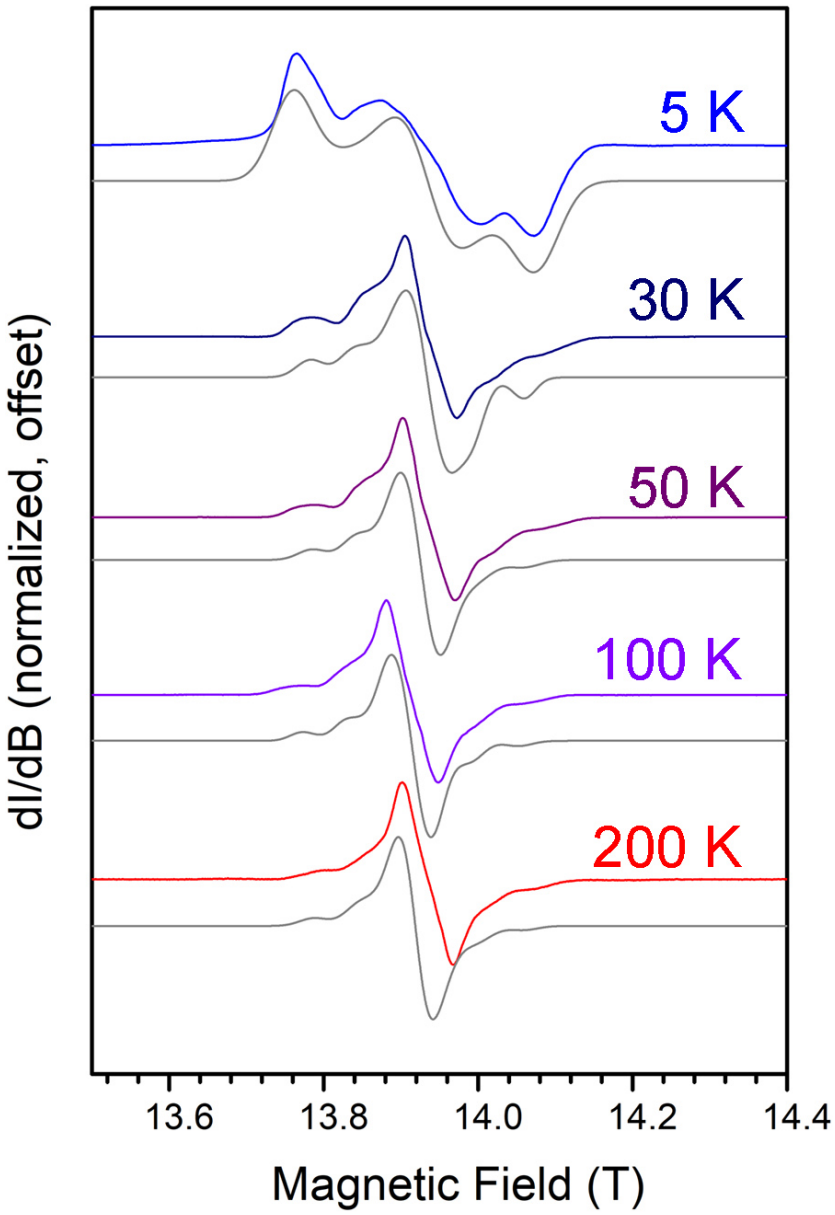

Fig. S9. Select variable-temperature 390 GHz solid-state EPR spectra for **3**. Colored lines correspond to the temperatures indicated on the graph. Gray lines are best simulations. Parameters for these simulations are listed in Table S6 and see the main manuscript for discussion.

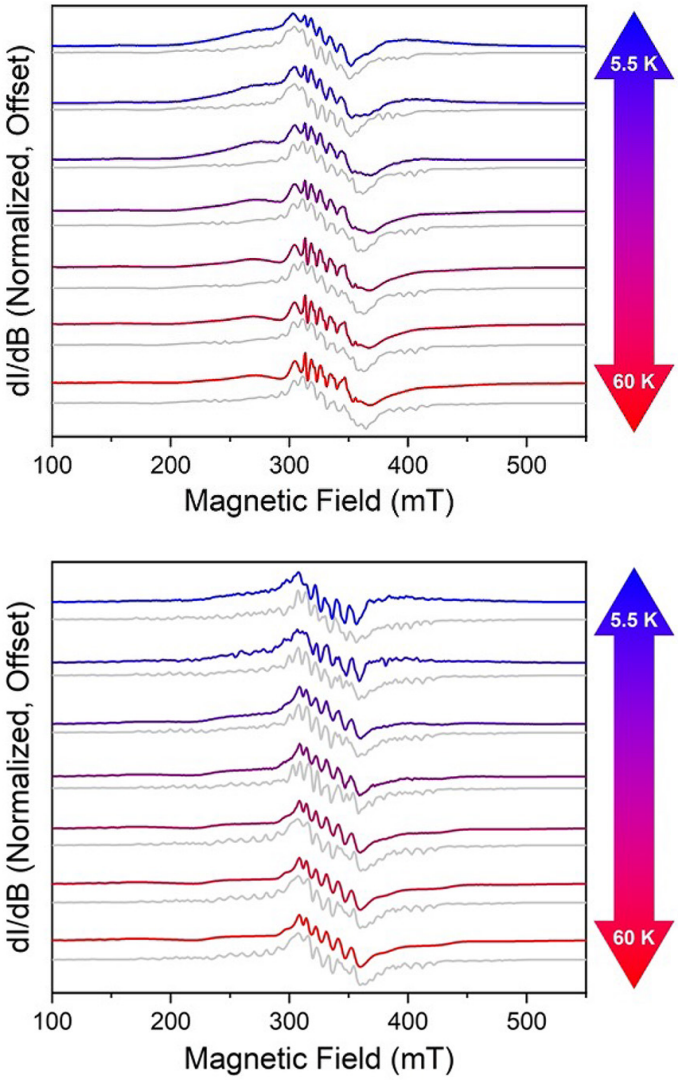

Fig. S10. Variable-temperature cw-EPR spectra of complex **1** (top) and **3** (bottom) collected from 5.5 K to 60 K at 9.3 GHz. Spectra were collected in 5 mM butryonitrile solutions.

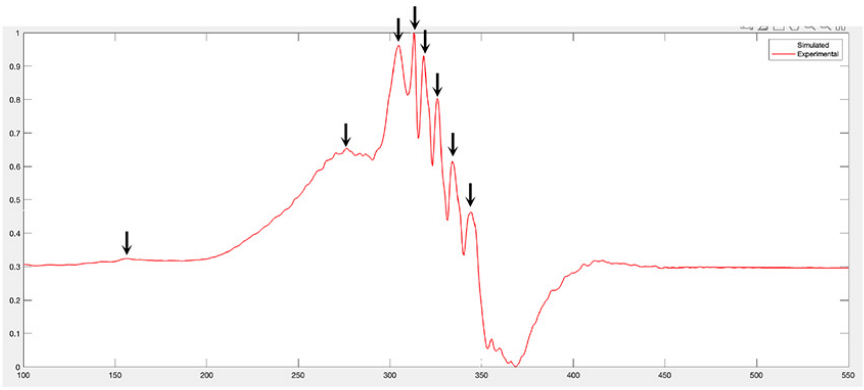

5.5 K	10 K	20 K	30 K	40 K	50 K	60 K
156.172	155.7	156.17	155.2	155.19	156.2	156.66
-	-	276.77	272.87	267.988	269.5	271.4
302.656	304.121	304.6	304.6	304.121	304.121	304.121
312.91	312.91	312.91	312.91	313.398	313.398	313.398
318.281	318.281	318.281	318.7	318.3	318.281	318.77
325.6	325.6	325.6	326	326	325.6	326.09
334.4	333.9	333.9	334.4	333.906	333.906	333.906
343.7	343.2	343.67	344.16	344.648	346.602	346.602

Fig. S11. Temperature dependence of peak positions for compound **1** in frozen solution. **Top:** 20 K X-band EPR spectrum for **1**. Black arrows indicate selected peaks for monitoring. **Bottom:** Table of peak positions (in mT) for the indicated peaks as a function of temperature. Empty boxes indicate temperatures where the peak was indistinguishable from background.

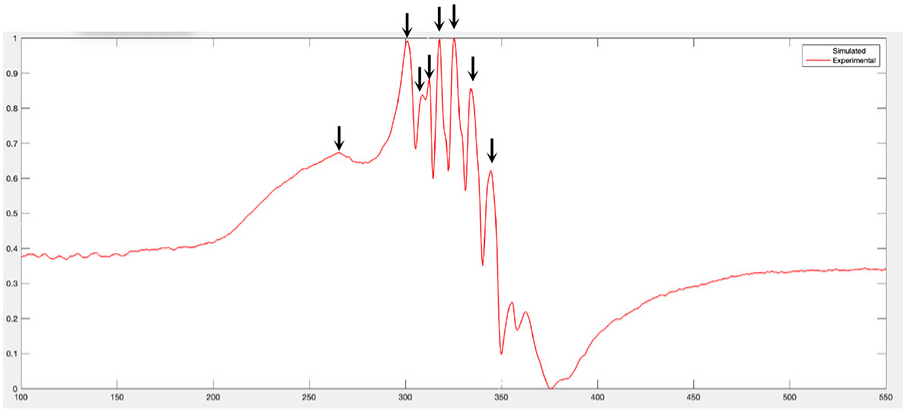

10 K	20 K	30 K	40 K	50 K
	265.059	263.594	263.594	264.08
300.703	300.703	300.703	300.703	300.703
309.492	309.004	309.004	309.004	
312.422	312.422	311.934	311.45	311.934
317.793	317.793	317.793	317.793	317.793
325.117	325.117	325.117	325.603	325.605
333.906	333.906	333.906	334.88	334.395
344.16	344.16	344.6	344.7	334.648

Fig. S12. Temperature dependence of peak positions for compound **2** in frozen solution. **Top:** 20 K X-band EPR spectrum for **2**. Black arrows indicate selected peaks for monitoring. **Bottom:** Table of peak positions (in mT) for the indicated peaks as a function of temperature. Empty boxes indicate temperatures where the peak was indistinguishable from background.

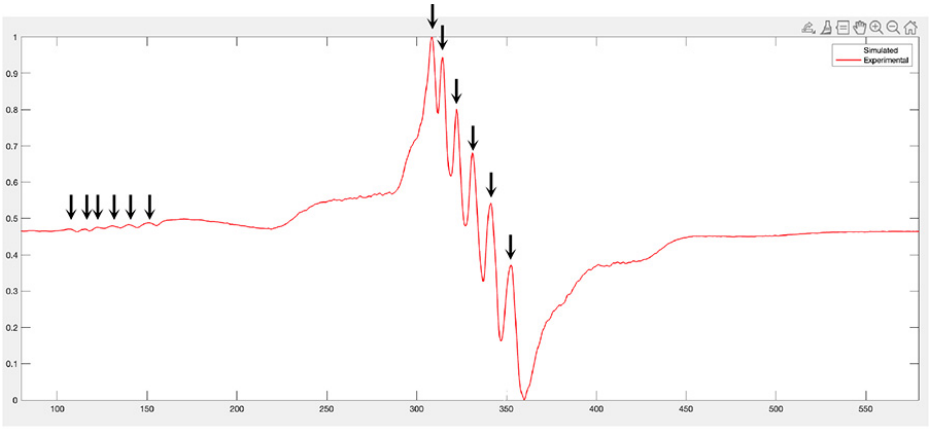

5.5 K	10 K	20 K	30 K	40 K	50 K
106.855	106.855	106.367	106.855	106.367	106.367
114.668	114.668	114.668	115.156	115.156	114.668
122.48	121.992	122.48	121.992	121.992	121.504
130.781	130.781	130.293	130.293	130.781	130.293
140.059	139.57	139.57	139.57	139.57	139.57
150.801	151.777	150.801	150.313	150.801	150.801
297.285	295.3	-	-	-	-
307.051	306.56	308.027	308.516	308.516	308.516
-	-	314.375	314.375	314.375	314.375
321.699	322.676	321.211	322.676	322.188	322.188
329.512	331.465	331.953	330.977	330.977	331.465
339.766	341.719	340.254	340.742	341.719	341.23
350.508	352.949	351.973	351.484	351.937	351.973

Fig. S13. Temperature dependence of peak positions for compound **3** in frozen solution. **Top:** 40 K X-band EPR spectrum for **3**. Black arrows indicate selected peaks for monitoring. **Bottom:** Table of peak positions (in mT) for the indicated peaks as a function of temperature. Empty boxes indicate temperatures where the peak was indistinguishable from background.

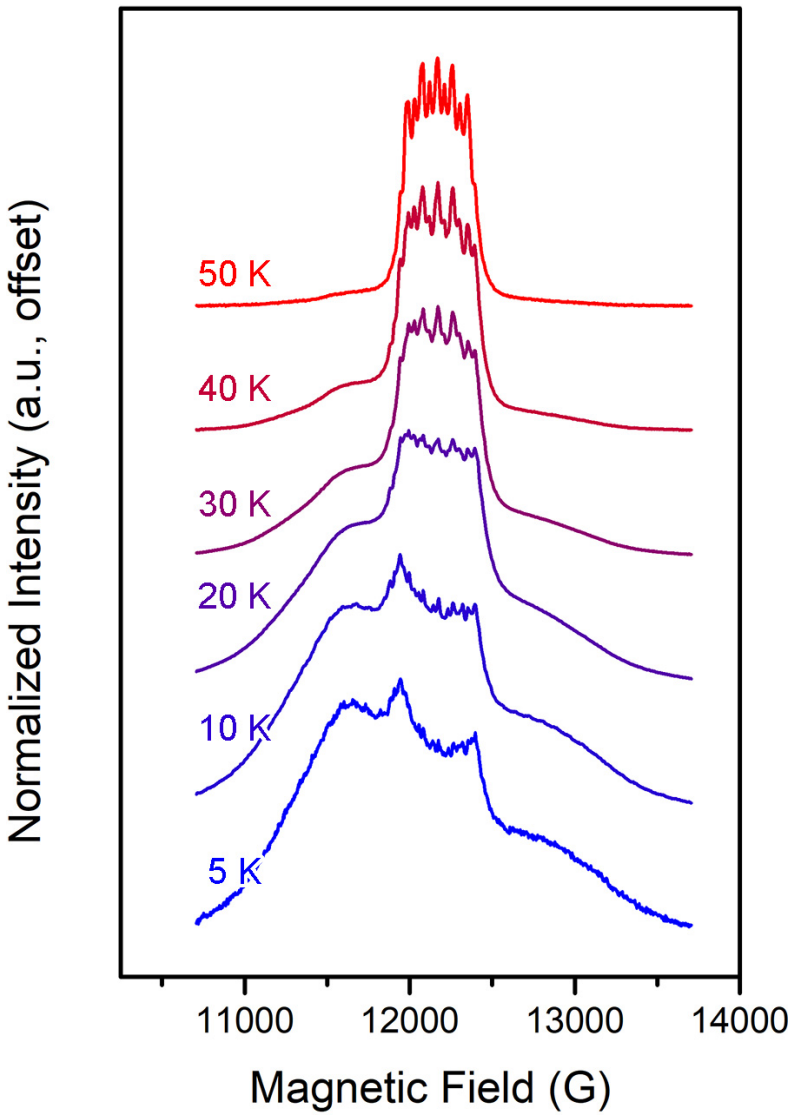

Fig. S14. Variable-temperature Q-band echo-detected EPR spectra for **2** in frozen butyronitrile solution. Concentration was 5 mM, 10 ns $\pi/2$ and 20 ns π pulses with 200 ns interpulse spacing.

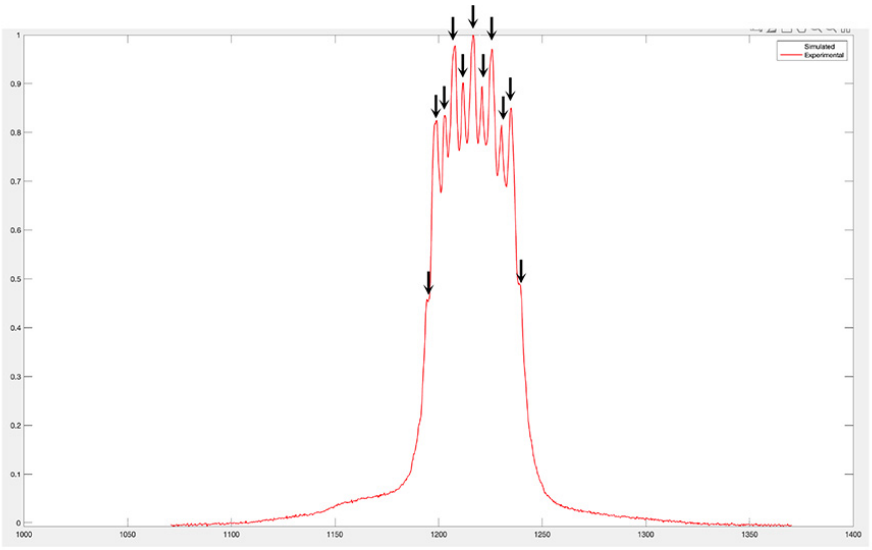

10 K	20 K	30 K	40 K	50 K
1193.85	1194.43	1194.43	1194.14	1194.43
1199.41	1199.71	1199.12	1199.12	1198.83
1202.93	1202.34	1202.64	1202.93	1203.22
1208.20	1208.50	1208.20	1207.91	1207.62
1214.35	1211.72	1211.72	1211.42	1212.01
1217.28	1216.99	1216.99	1216.99	1216.70
1222.85	1220.80	1220.80	1220.51	1221.09
1225.78	1225.78	1225.78	1225.78	1225.78
1231.93	1229.59	1230.17	1229.59	1230.17
1235.45	1234.86	1235.16	1235.16	1235.16
1239.26	1239.26	1239.26	1239.26	1239.26

Fig. S15. Temperature dependence of Q-band EPR peak positions for compound **2** in frozen solution. **Top:** 50 K Q-band echo-detected EPR spectrum for **2**. Black arrows indicate selected peaks for monitoring. **Bottom:** Table of peak positions (in mT) for the indicated peaks as a function of temperature. Empty boxes indicate temperatures where the peak was indistinguishable from background.

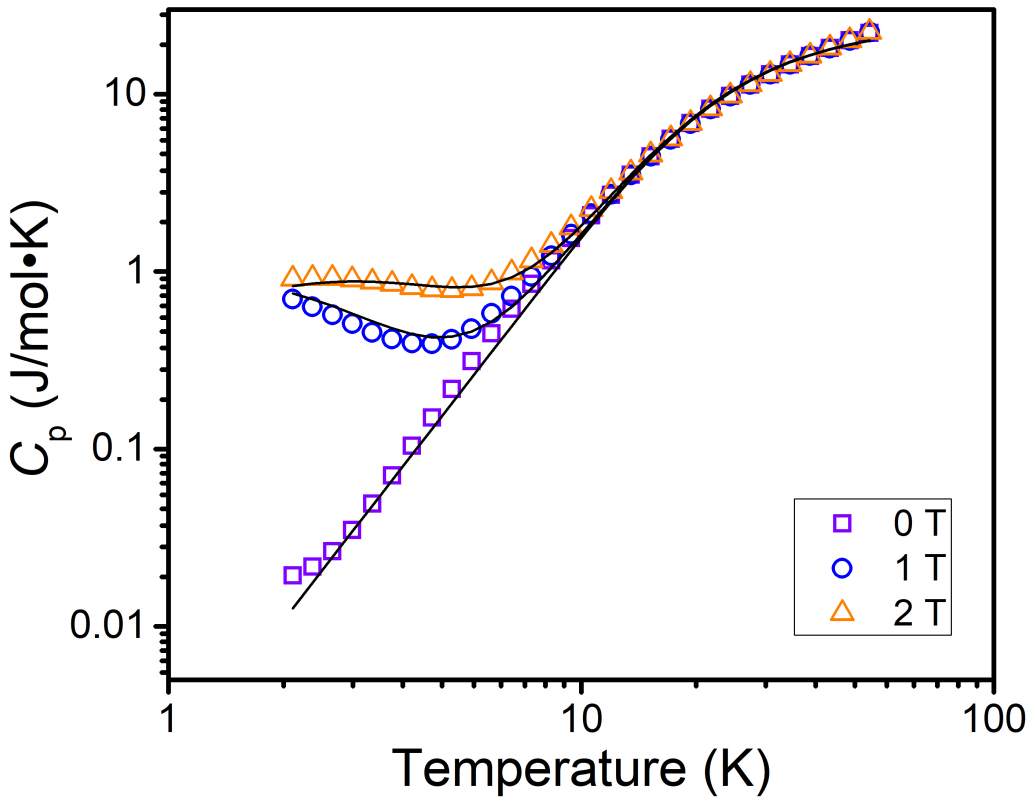

Fig. S16. Field and temperature-dependence of the heat capacity of **2** measured from 2 to 50 K. Solid lines are simulations of the heat capacity, see main text for details.

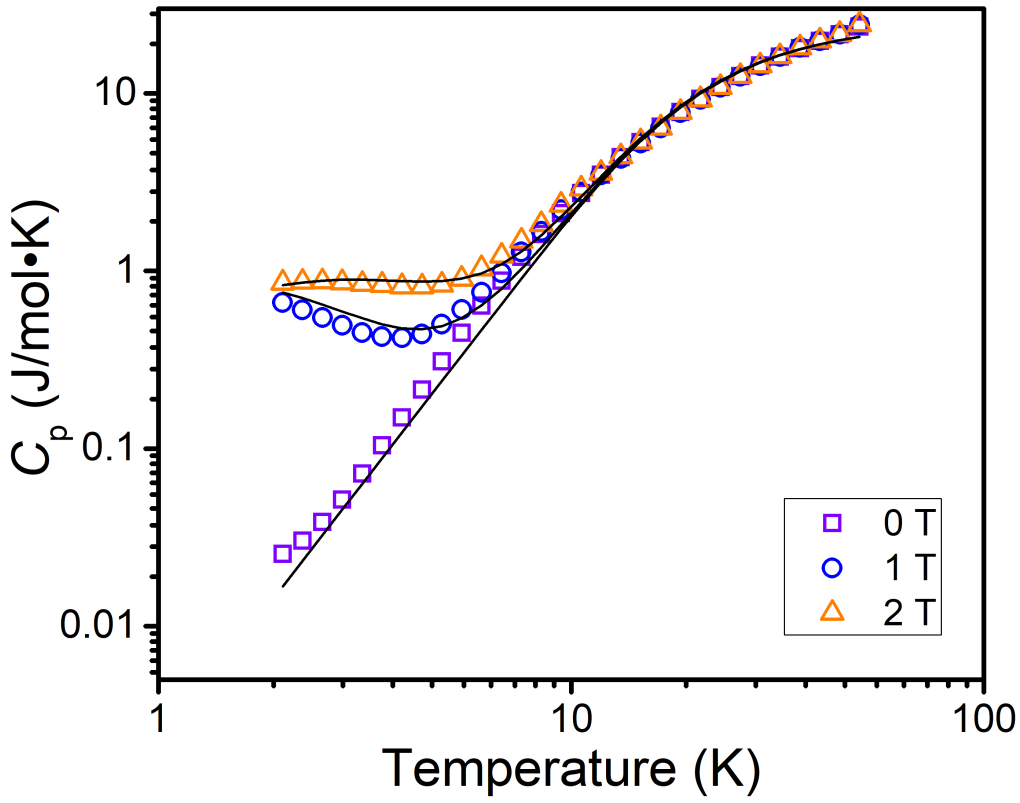

Fig. S17. Field and temperature-dependence of the heat capacity of **3** measured from 2 to 50 K. Solid lines are simulations of the heat capacity, see main text for details.

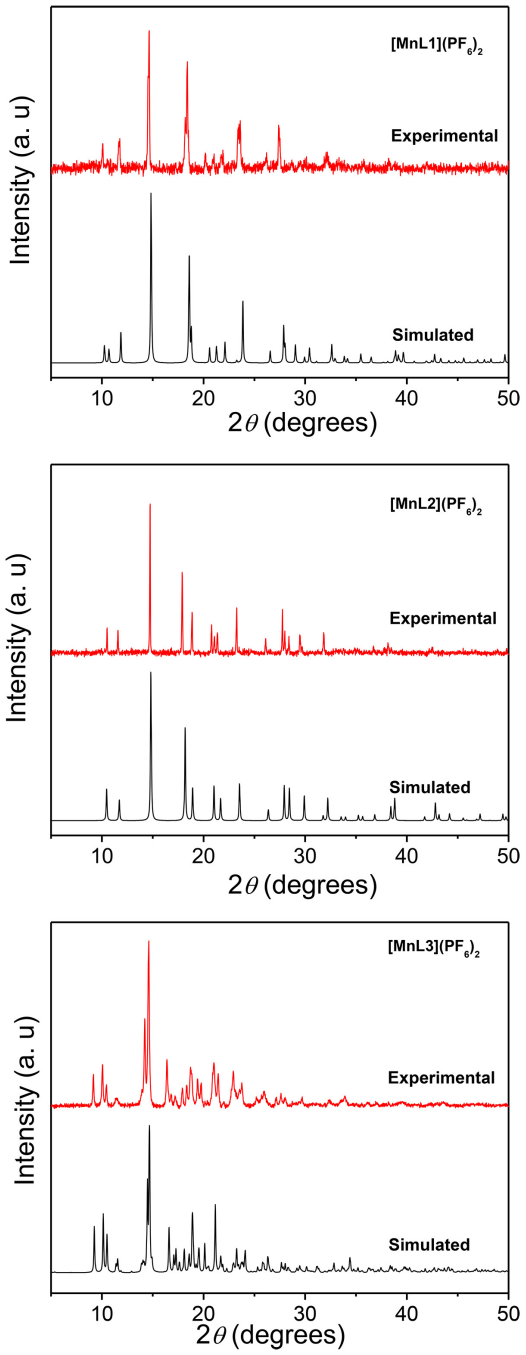

Fig. S18. Powder diffraction patterns for **1**(top), **2**(middle), and **3**(bottom). The red plot is experimental data, the black simulations represent diffraction patterns simulated from the results of single-crystal diffraction experiments by Mercury.